Korean J. Chem. Eng., 33(10), 3029-3034 (2016)
DOI: 10.1007/s11814-016-0170-y

pISSN: 0256-1115
eISSN: 1975-7220

Manganese oxides nanocrystals supported on mesoporous carbon microspheres for energy storage application

Dae-Hoon Yeom, Jaeho Choi, Woo Jin Byun, and Jung Kyoo Lee†

Department of Chemical Engineering, Dong-A University, Busan 49315, Korea
(*Received 27 January 2016 • accepted 20 June 2016*)

Abstract−Mesoporous carbon microspheres (MCM) with a uniform size distribution (1-2 μm in diameter) were replicated from mesoporous silica microspheres (MSM) by using sucrose as a carbon source. MCM (BET surface area=1,001 m^2/g, total pore volume=0.82 cc/g, average pore size=3.4 nm) was used as the support of MnO_x nanocrystals (Mn_3O_4 with MnO as a minor phase). The MnO_x/MCM composite was prepared by pore-filling wet-impregnation of Mn nitrate solution followed by a moderate annealing under Ar flow. Thus obtained MnO_x/MCM composite was characterized as a high capacity anode for lithium ion battery (LIB). The electrochemical responses of MnO_x/MCM were investigated in comparison with those of commercial graphite. The MnO_x/MCM composite exhibited the reversible capacity of ~720 mAh g^{-1} at the current density of 200 mA g^{-1} with an excellent cycling stability up to 100 cycles. The MnO_x/MCM composite also showed much higher volumetric capacity and better rate capability than the state of the art graphite anode, suggesting its potential use as a new anode material for LIBs.

Keywords: Lithium-ion Battery, Anode, Manganese Oxide, Mesoporous Carbon Microsphere, Transition Metal Oxide

INTRODUCTION

Lithium-ion batteries (LIBs) as energy storage devices are in great demand due to their widespread industrial applications such as micro-medical devices, wireless electronic devices and electrical tools, high-energy/high-power electrified vehicles and energy storage systems (ESS) of various scales [1-4]. However, current anodes based on graphitic carbon cannot meet the increasing demands for high energy and power densities due to its low theoretical specific capacity (372 mAh g^{-1} with one Li per C_6) and very poor rate capability arising from the low intrinsic Li intercalation rate into its lattice crystal structure (d=3.35 Å), respectively [5].

Since the first introduction by Poizot et al. in 2000, transition metal oxides (TMOs such as FeO_x and MnO_x etc.) have been extensively studied as promising anode materials to replace graphitic carbon [6-14]. That is because TMOs can deliver high capacity (750-1,200 mAh g^{-1}) by the electrochemical "conversion reaction"" given in Eq. (1). Its forward reaction is thermodynamically favorable with high negative Gibbs free energy changes. However, its reverse reaction requires an external electromotive force (emf) greater than the equilibrium potential [15]. Thus, typically TMOs accompany voltage hysteresis between charging and discharging process in which the size of hysteresis is depending upon TMO species [11,15]. Nonetheless, TMOs, such as FeO_x and MnO_x are attractive anode materials because they are abundant, cheap and nontoxic. In addition, they have high intrinsic density (4.9-5.4 g cm^{-3} versus 2.16 g cm^{-3} for graphite) in favor of high volumetric energy density than graphitic carbon [5,12].

$$M_xO_y+2y\,(Li^+)+2y\,(e^-)\leftrightarrow x\,(M)+y\,(Li_2O) \quad (1)$$

Among TMOs, manganese oxides (MnO_x) are of particular interest owing to their lower equilibrium potential in the forward reaction in Eq. (1) above, smaller voltage hysteresis than other TMOs, and high capacity (756-1,223 mAh g^{-1}) depending upon their oxidation states [14]. To obtain higher capacity, MnO_x with higher oxidation states such as MnO_2 (1,233 mAh g^{-1}), Mn_2O_3 (1,018 mAh g^{-1}) and Mn_3O_4 (937 mAh g^{-1}) are more demanding than MnO (756 mAh g^{-1}). However, it is quite challenging to extract the corresponding theoretical capacities from MnO_x due to their intrinsic low electrical conductivity (~10^{-5}-10^{-8} S/cm) and drastic chemical and structural changes inherently accompanying the conversion reaction [16,17]. Hence, composites of MnO_x with conductive carbon material are generally adopted [5,8,18]. However, MnO_x reduction occurs during the carbonization of composite gel, which decreases the theoretical capacity of MnO_x/C composite since the oxidation states of Mn change, for example, from $Mn^{+(2\sim3)}$ (Mn_3O_4) to Mn^{+2} (MnO) [14]. Recently, we devised a bottom-up *in situ* synthesis method as an alternative approach to avoid TMOs reduction during their carbon coating process [5,12]. In the bottom-up synthesis, TMOs/C composite was prepared by a simple impregnation of aqueous TMO precursor solutions on the preformed mesoporous carbons followed by annealing at a moderate temperature. On the other hand, the energy density of an electrode can be enhanced by increasing the coating density of electrode material on current collector. Therefore, the morphology of active material is also important in this regard, and thus various mesoporous carbon microspheres were successfully employed in energy storage applications [18-21].

In this study, mesoporous carbon microspheres (MCM) with a uniform size distribution (1-2 μm in diameter) were prepared by employing mesoporous silica microspheres (MSM) as a template.

†To whom correspondence should be addressed.
E-mail: jklee88@dau.ac.kr

MCM was used as the support of MnO_x nanocrystals to prepare MnO_x/MCM composite. Thus prepared MnO_x/MCM composite was used as high capacity anodes for LIBs. The electrochemical responses of MnO_x/MCM were investigated by galvanostatic charge/discharge cycling and rate tests in comparison with those of commercial graphite anode. The MnO_x/MCM composite exhibited much higher reversible capacity (specific and volumetric) and better rate capability than the state of the art graphite anode. It also showed an excellent cycling stability up to 100 cycles.

EXPERIMENTAL

1. Synthesis of MSM and MCM

The mesoporous silica microsphere (MSM) was prepared according to the previous report [21]. In a typical preparation, *n*-octadecylamine (2.0 g, ≥99%, Sigma-Aldrich) was dissolved in a mixture of deionized (DI) water (172 mL), isopropanol (200 mL) and NH_4OH (20-30%, 3.2 mL). The mixture was stirred at 500 rpm for 2 h to form a homogeneous solution. Then, tetraorthosilicate (TEOS, 12 mL) was added to the mixture and the mixture was stirred at 35 °C for 12 h. The solid product was filtered, washed with DI water and dried in air at 80 °C overnight. To remove the surfactant, dried product was calcined in air at 600 °C for 6 h.

In a typical preparation of mesoporous carbon microsphere (MCM), MSM (1.0 g) was well dispersed in an aqueous mixture consisting of DI water (5.0 mL), H_2SO_4 (0.14 g) and sucrose (1.25 g). The viscous mixture was dried in a well-ventilated fume hood at 100 °C for 12 h, and then the sample was further heated at 160 °C for 6 h. Thus obtained sample was mixed again with an aqueous mixture of DI water (5.0 mL), H_2SO_4 (0.08 g) and sucrose (0.75 g), and was subjected to the same drying procedure as above [22]. The dried sample was carbonized in a tube furnace in Ar flow at 850 °C for 2 h. The recovered sample was dispersed in 15 wt% HF solution in a Teflon tube and subjected to sonication to dissolve MSM template. The product was filtered, washed with DI water and dried to obtain MCM.

2. Preparation of MnO_x/MCM Composite

The MnO_x/MCM composite was prepared by a pore-filling wet impregnation method described elsewhere [5,7,12]. In a typical preparation, a saturated Mn precursor solution was prepared by dissolving $Mn(NO_3)_2{\cdot}5H_2O$ in acetone. An amount of Mn solution, equivalent to the pore volume of MCM determined by the BET measurement, was impregnated onto MCM and the Mn-impregnated MCM was dried in air at 80 °C. This process was repeated several times until the desired amount of Mn precursor was loaded on MCM. After drying, the sample was heated in an Ar flow at 450 °C for 2 h to obtain MnO_x/MCM.

3. Materials Characterization

The powder X-ray diffraction (XRD) patterns of sample were collected on an Ultima IV, Rigaku model D/MAX-50 kV system (Cu-Kα radiation, λ=1.5418 Å). The MnO_x content in MnO_x/MCM composite was estimated by the weight loss due to carbon oxida-

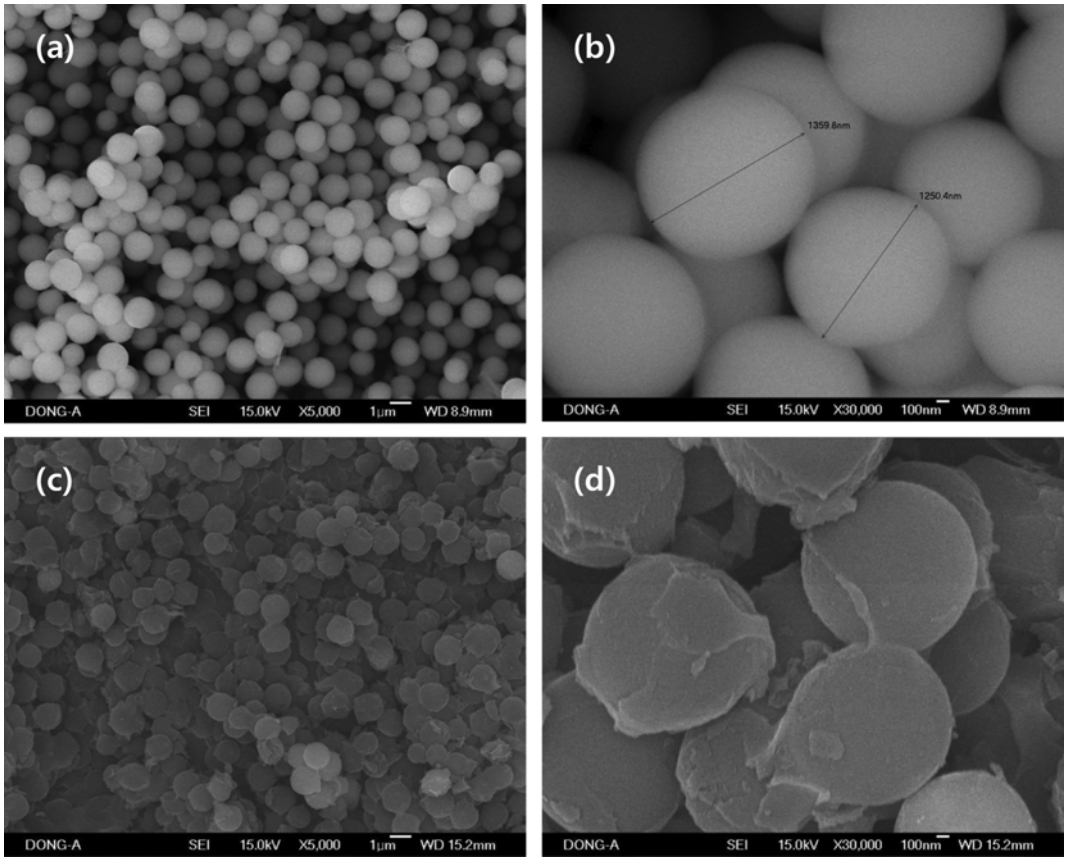

Fig. 1. SEM images of (a), (b) mesoporous silica microspheres (MSM) and (c), (d) mesoporous carbon microspheres (MCM).

tion in a TGA run to 800 °C in air flow. The morphology and structure of samples were investigated with SEM (JEOL JSM-35CF operated at 10.0 kV, JEOL Ltd., Japan) and TEM (JEOL JEM-2010 operated at 200.0 kV, JEOL Ltd., Japan). Nitrogen adsorption-desorption isotherms were obtained at liquid N_2 temperature using a Micromeritics ASAP 2000 to estimate BET surface areas, and pore sizes and pore-size distributions of samples. Raman spectrum was measured on a Renishaw Raman spectrometer using a laser of 632.8 nm.

4. Electrochemical Measurements

The electrochemical responses were measured using R-2016 coin cell with Li foil as the reference electrode. The working electrodes (35-40 μm thick) were prepared by casting a paste consisting of 80 : 10 : 10 in wt% of active material (MCM, MnO_x/MCM or graphite), conductive additive (Super P Li, TIMCAL Ltd.) and binder, respectively, on a copper foil. Polyvinylene acetate (PVA) and Polyvinylidene fluoride (PVDF) were used as the binder for MnO_x/MCM and graphite, respectively. A polypropylene membrane (Celgard 2400) was used as the separator. 1.0 M $LiPF_6$ dissolved in an ethylene carbonate/dimethyl carbonate/diethyl carbonate (EC/DMC/DEC) mixture (3 : 4 : 3 v/v/v) (PANAX ETECH Ltd., Korea) containing 5 vol% of fluoroethylene carbonate (FEC) was used as the electrolyte for MnO_x/MCM. The cells were assembled in an argon-filled glove box and cycled with the cut-off voltage range of 0.01-3.0 V vs. Li^+/Li on a galvanostat/potentiostat system (WonATech, Korea).

RESULTS AND DISCUSSION

Fig. 1 presents the SEM images of MSM and MCM. MSM particles show spherical morphology with a uniform size distribution in the range of 1.2-1.4 μm (Fig. 1(a) and (b)). In Fig. 1(c) and (d), MCM particles derived from MSM template also show spherical shapes with particle size distribution similar to that of MSM, suggesting that MCM was successfully replicated from MSM as the template. However, MCM particles show a rather rough surface compared to MSM, possibly due to slightly excessive use of sucrose as the carbon precursor.

In Figs. 2(a) and (b), N_2 adsorption/desorption isotherms and pore size distributions of MSM, MCM and MnO_x/MCM are compared, respectively. The isotherm curves of MSM reached a virtual plateau at P/P_0=0.4 without showing a distinct adsorption/desorption hysteresis loop. This indicates that MSM has fairly small pores and its pore size distribution is quite narrow, which is consistent with its pore size distribution (1.7-3.7 nm) shown in Fig. 2(b). On the other hand, MCM exhibited much larger amount of N_2 adsorption than MSM. MCM also showed a distinct hysteresis loop at P/P_0=0.4-0.8 with a wide range of pore size distribution (1.7-8.5 nm). As a result, MCM has much larger BET surface area (1,001 m^2/g) and total pore volume (0.82 cc/g) than MSM (658 m^2/g, 0.53 cc/g) as compared in Table 1. The average pore diameters of MSM and MCM were 2.6 and 3.4 nm, respectively. The textual properties of MCM determined by BET measurement were comparable to those of an ordered mesoporous carbon (OMC) [5]. The amount of N_2 adsorbed on MnO_x/MCM was much lower than that on MCM. The distinct nitrogen adsorption-desorption hysteresis on the isotherms of MCM was merely observed on MnO_x/MCM.

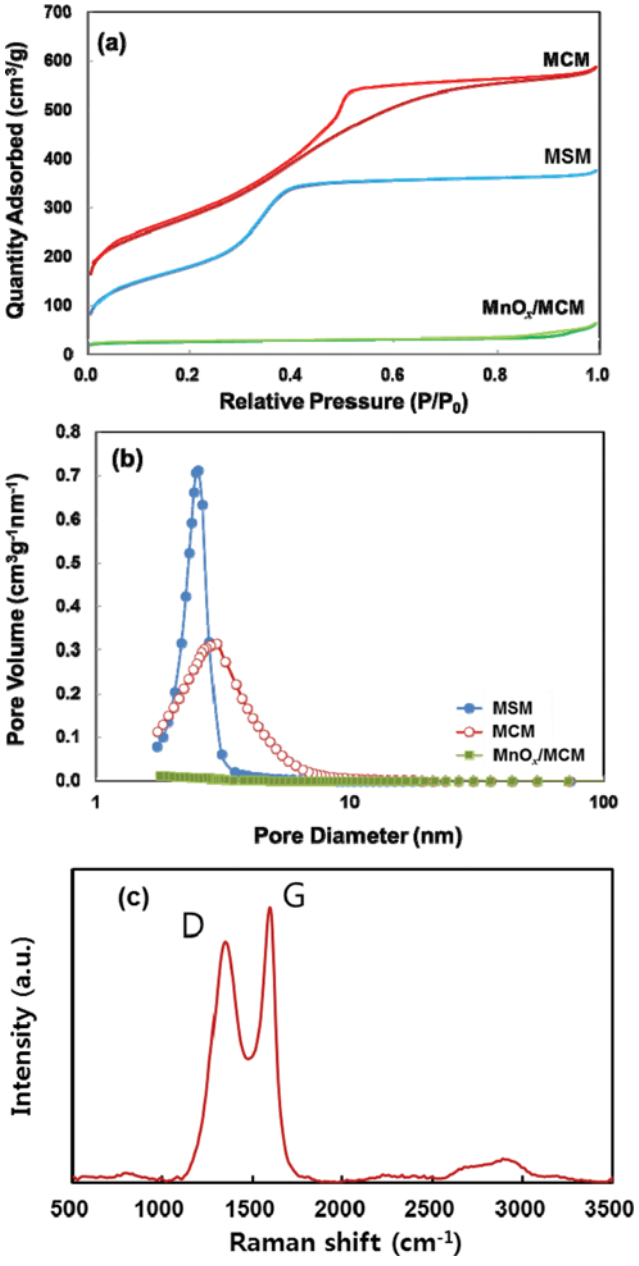

Fig. 2. (a) Nitrogen adsorption/desorption isotherms, (b) pore size distributions of MSM, MCM and MnO_x/MCM and (c) Raman spectrum of MCM.

Table 1. Textual properties of MSM, MCM and MnO_x/MCM

	MSM	MCM	MnO_x/MCM
BET S_A (m^2/g)	657.8	1001.2	102.4
V_{pore} (cc/g)	0.53	0.82	0.07
D_{pore} (nm)	2.6	3.4	n. a.

Furthermore, MnO_x/MCM showed much lower BET surface area (102 m^2/g) and total pore volume (0.07 cm^3/g) than bare MCM as compared in Table 1. These results support that most of small MnO_x nanocrystals are located in the meso-pores of MCM. Fig. 2(c) shows the Raman spectrum of MCM with two intense peaks at around

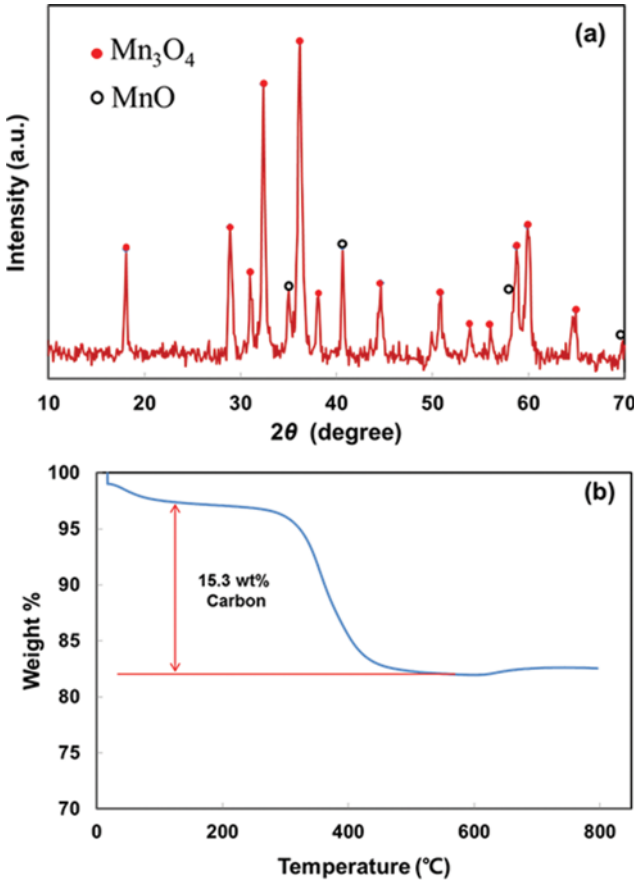

Fig. 3. (a) XRD pattern and (b) TGA profile of MnO_x/MCM.

1,348 and 1,596 cm^{-1}, corresponding to the D band for disordered graphite or crystal defects and the G band for an ideal graphitic structure of the carbon plane, respectively. The relative intensity ratio of the D band and the G band (I_D/I_G) for MCM was 0.87, indicating that MCM has partial graphitic layers in mainly disordered graphite matrix.

The XRD pattern of MnO_x/MCM shown in Fig. 3(a) reveals that Mn_3O_4 was formed as a major structure with a small portion of MnO impurity phase. In our previous report [14], MnO (Mn^{2+}) was formed as a major phase by following a carbon coating process for pre-formed Mn_3O_4 nanocrystals due to the reduction of Mn_3O_4 to MnO during carbonization process. Hence, manganese oxides with a higher oxidation state than MnO (Mn^{2+}) can be formed by following the bottom-up *in situ* formation of MnO_x nanocrystals in a preformed mesoporous carbon. From the TGA profile in Fig. 3(b), the amount of MnO_x in MnO_x/MCM was estimated to be 84.7 wt%. Fig. 4 shows the TEM image of MnO_x/MCM. MnO_x particles in the range of 3-30 nm in size were formed on MCM and large MnO_x particles formed in MCM pores may partly destroy the pore structure of MCM during the thermal annealing, which was also observed on ordered mesoporous carbons [5,23]. As shown in the inset of Fig. 4, a fair amount of MnO_x particles were found near the external surfaces of MCM with some fracture of MCM due to the heavy MnO_x loading on MCM which can cause particle growth during the thermal annealing process.

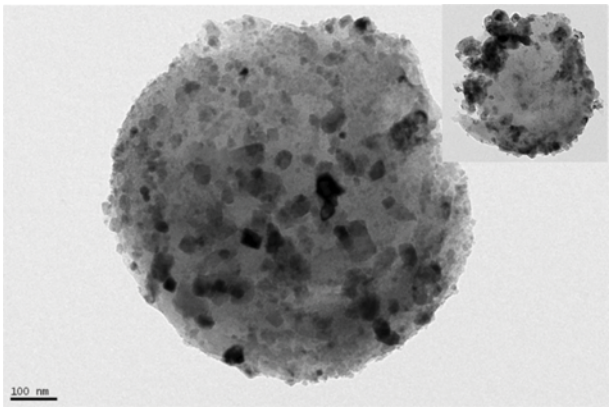

Fig. 4. TEM image of MnO_x/MCM.

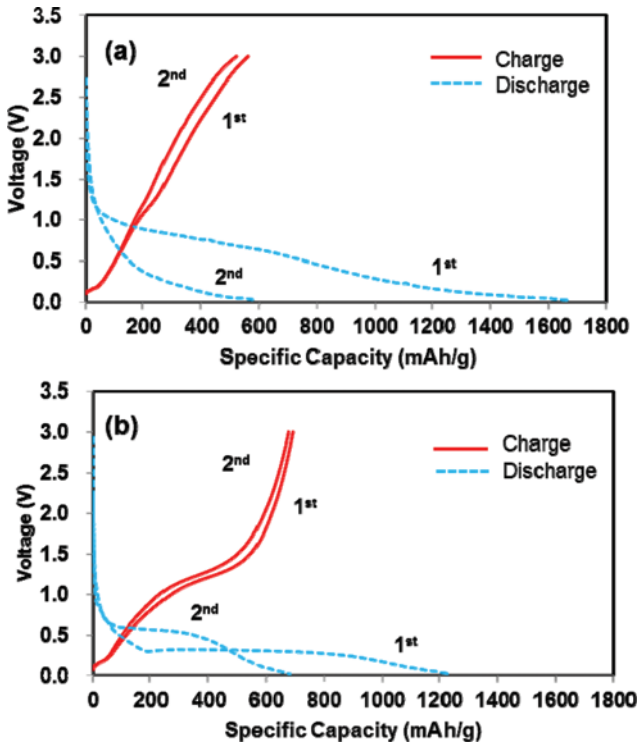

Fig. 5. Charge/discharge voltage profiles of (a) MCM and MnO_x/MCM at the current of 100 mA g^{-1}.

Fig. 5 displays the charge/discharge voltage profiles of bare MCM and MnO_x/MCM for the initial two cycles at a current density of 100 mA g^{-1}. The bare MCM showed the first discharge (lithiation) and charge (de-lithiation) capacities of 1,670 and 563 mAh g^{-1}, respectively, giving the Coulombic efficiency (CE) of only 33.7% in the first cycle. The reversible discharge capacity in the second cycle was 589 mAh g^{-1} with the corresponding CE of 88.6%. The bare MCM exhibited much larger reversible capacity than graphite due to the extra lithium storage in the micro- and mesopores of MCM as typically observed in porous carbon materials [24]. However, it showed a large voltage hysteresis between the charge-discharge processes without distinct potential plateaus. The MnO_x/MCM showed the first discharge and charge capacities of 1,230 and 692 mAh g^{-1}

with the first CE of 56.3%. The reversible discharge capacity in the second cycle was 682 mAh g^{-1} with the corresponding CE of 99.3%. In the first discharge profile of MnO_x/MCM, a sloping voltage plateau corresponding to discharge capacity of around 170 mAh g^{-1} was observed at 0.9-0.3 V vs. Li^+/Li, but it almost disappeared in the subsequent cycles suggesting irreversible lithium storage associated with electrolyte decomposition forming a solid-electrolyte interface (SEI) layer [25]. Different from MCM, MnO_x/MCM showed a long and distinct voltage plateau at around 0.3 V vs. Li^+/Li due to the electrochemical reduction of MnO_x (Mn^{3+} and Mn^{2+}) to Mn^0 and Li_2O. It is obvious that the lithium storage voltage of MnO_x (around 0.3 V vs. Li^+/Li) is much lower than that of FeO_x (around 0.8 V vs. Li^+/Li) [12]. In addition, a sloping voltage profile down to 0.01 V vs. Li^+/Li was recorded due to the interfacial lithium storage in the nano-grain boundaries of Mn and Li_2O [5,26]. In the subsequent discharge cycles, the obvious plateau at around 0.3 V was shifted to above 0.5 V due to electrode polarization caused by an abrupt phase transition between polycrystalline MnO_x and Mn/Li_2O nano-domains [14,27]. In the charge profiles of MnO_x/MCM, sloping voltage plateaus were observed at 0.8-1.3 V due to the oxidation of Mn^0 to Mn^{2+}/Mn^{3+} according to reaction (1) above [5,7].

Fig. 6 presents the cycling performances of MCM and MnO_x/MCM in comparison with that of commercial graphite. After initial three cycles at the current density of 100 mA g^{-1}, all the samples were cycled at 200 mA g^{-1} up to 100 cycles. The specific and volumetric capacities are compared in Fig. 6(a) and (b), respectively. At 200 mA g^{-1}, MnO_x/MCM exhibited specific discharge capacities of around 600 mAh g^{-1} and showed excellent cycling stability up to 100 cycles. After the 50th cycle on, the discharge capacities gradually increased with cycle number to reach 720 mAh g^{-1} at the end of cycle. The increasing capacity of various TMOs with cycle number was reported to be associated with the formation of high oxidation state products or gel-like polymeric films due to electrolyte degradation [28,29]. At 200 mA g^{-1}, MCM exhibited specific discharge capacity of around 380 mAh g^{-1} at the beginning and showed 262 mAh g^{-1} at the end of cycle, giving a capacity retention of 68.9%. At 200 mA g^{-1}, graphite showed a gradual increase in the specific discharge capacities in the range of 223-343 mAh g^{-1} up to the 40th cycle, and the capacities were stabilized in the range of 342-347 mAh g^{-1} up to the end of the cycle. Hence, MnO_x/MCM composite delivered almost twice the capacity of graphite, and it also showed excellent cycling stability up to 100 cycles. For lighter LIB fabrication, an anode material having higher specific capacity is demanded. It is also highly desirable to compare the volumetric capacity of an anode material to that of commercial graphitic carbon anode. In this aspect, the volumetric capacities of electrodes are compared in Fig. 6(b). The volumetric capacity (mAh cm^{-3}) of an electrode was calculated as follows: [specific capacity, mAh g^{-1}]×[(electrode weight inclusive of active material, binder and conductive additive)/(electrode volume), g cm^{-3}]. At a current of 100 mA g^{-1}, the volumetric capacities of MnO_x/MCM and graphite were 992-994 and 563-569 mAh cm^{-3}, respectively. Therefore, the MnO_x/MCM exhibited about 1.7-times higher volumetric capacity than graphite. The theoretical volumetric capacity of graphite would be about 803.5 mAh cm^{-3} [(372 mAh g^{-1} (theoretical specific capacity))×(2.16 g cm^{-3} (density of graphite))]. However, the actual volumetric capacity of graphite electrode was found to be lower than the theoretical one, since the total electrode volume including all the components (active material, binder and conductive additive) in the electrode was counted for volumetric capacity. At the end of cycle at 200 mA g^{-1}, the MnO_x/MCM showed the volumetric capacity of 1,049 mAh cm^{-3}, which was almost twice the volumetric capacity of graphite (533 mAh cm^{-3}). The high volumetric capacity of MnO_x/MCM can be ascribed to the intrinsic high density of MnO_x (4.86 and 5.43 g/cm^3 for Mn_3O_4 and MnO, respectively) and the spherical morphology of MCM with a uniform size of about 1.3 μm on aver-

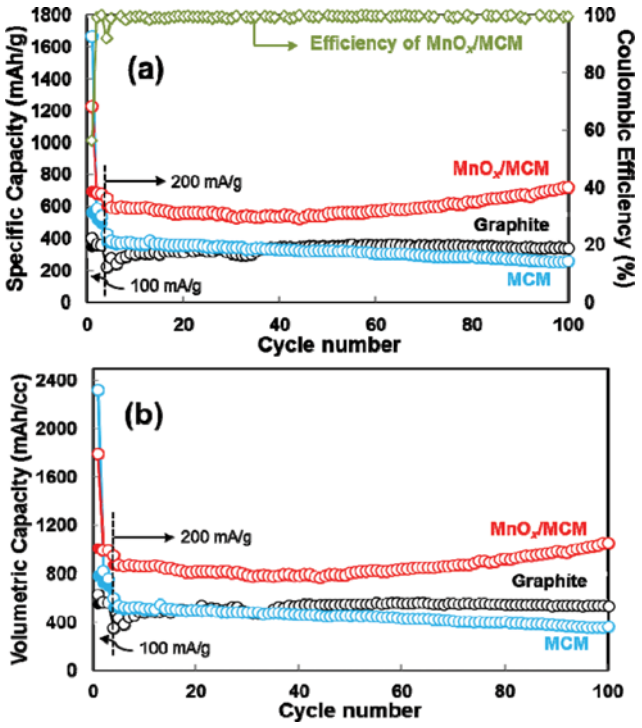

Fig. 6. (a) Specific and (b) volumetric capacities of graphite, MCM and MnO_x/MCM with cycle number (open and filled symbols denote for discharge and charge capacities, respectively).

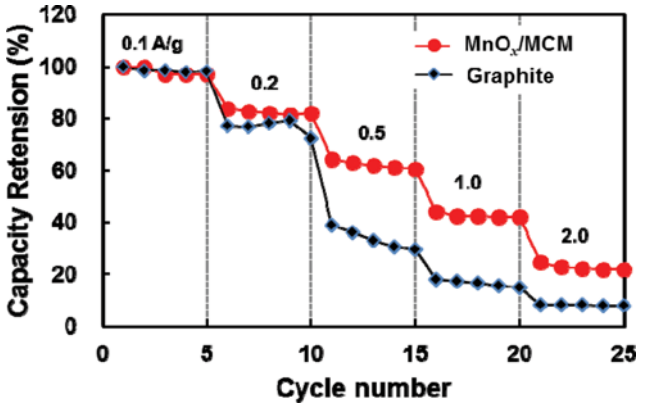

Fig. 7. Comparison of rate responses of graphite and MnO_x/MCM when both charge and discharge currents are varied at the same time in the range of 0.1-2.0 A g^{-1}.

age, which gives high coating densities of electrodes.

Fig. 7 displays the rate responses of MnO_x/MCM and graphite obtained by a step-wise increase of current density from 0.1 to 2.0 A g^{-1}. The capacity retention reported here is the charge capacities at different current density relative to that obtained at 0.1 A g^{-1}. Both samples exhibited similar level of capacity retention up to the current of 0.2 A g^{-1}. At the current of 0.5 A g^{-1}, however, the capacity retention of graphite was only 29-39%, while that of MnO_x/MCM was as high as 60-64%. Even at the current of 1.0 A g^{-1}, MnO_x/MCM showed the capacity retention level of 42-44% while graphite lost most of its capacity. These results suggest that the kinetics of electrochemical conversion reaction of MnO_x with lithium is more favorable than the conventional lithium intercalation/de-intercalation between the structural layers of graphite at high current density.

CONCLUSIONS

Mesoporous carbon microsphere (MCM) was successfully replicated from mesoporous silica microsphere, and the MCM possessed attractive textual properties of high surface area and large pore volume. MCM was used as a conducting support of transition metal oxides for LIB anodes. MnO_x (composed of Mn_3O_4 as the major phase with MnO as an impurity phase) nanocrystals were formed on MCM by a simple pore-filling wet-impregnation of Mn precursor solution followed by annealing at 450 °C in Ar flow. Thus obtained MnO_x/MCM composite exhibited about twice the capacity of commercial graphite anode at 200 mA g^{-1} with an excellent cycling stability up to 100 cycles. The MnO_x/MCM also showed much higher volumetric capacity and better rate capability than commercial graphite anode. Thus, the MnO_x/MCM composite could be an attractive candidate as a new anode material in LIBs requiring much higher volumetric as well as specific capacity than graphite.

ACKNOWLEDGEMENTS

This work was supported by the National Research Foundation of Korea Grant funded by the Ministry of Education, Science and Technology (NRF-2012R1A1A2042487) and by the Human Resource Training Program for Regional Innovation and Creativity through the Ministry of Education and National Research Foundation of Korea (NRF-2014H1C1A1073093).

REFERENCES

1. M. M. Thackeray, C. Wolverton and E. D. Isaacs, *Energy Environ. Sci.*, **5**, 7854 (2012).
2. B. Scrosati and J. Garche, *J. Power Sources*, **195**, 2419 (2010).
3. J. M. Tarascon, *Philos. Trans. R. Soc. A-Math. Phys. Eng. Sci.*, **368**, 3227 (2010).
4. M. S. Whittingham, *MRS Bull.*, **33**, 411 (2008).
5. C. Chae, J. H. Kim, J. M. Kim, Y. K. Sun and J. K. Lee, *J. Mater. Chem.*, **22**, 17870 (2012).
6. T. Yoon, J. Kim, J. Kim and J. K. Lee, *Energies*, **6**, 4830 (2013).
7. C. Chae, H. Park, D. Kim, J. Kim, E. S. Oh and J. K. Lee, *J. Power Sources*, **244**, 214 (2013).
8. Y. F. Deng, L. N. Wan, Y. Xie, X. S. Qin and G. H. Chen, *RSC Adv.*, **4**, 23914 (2014).
9. L. Li, Z. Guo, A. Du and H. Liu, *J. Mater. Chem.*, **22**, 3600 (2012).
10. H. Wang, L.-F. Cui, Y. Yang, H. S. Casalongue, J. T. Robinson, Y. Liang, Y. Cui and H. Dai, *J. Am. Chem. Soc.*, **132**, 13978 (2010).
11. J. Cabana, L. Monconduit, D. Larcher and M. R. Palacin, *Adv. Mater.*, **22**, E170 (2010).
12. T. Yoon, C. Chae, Y. K. Sun, X. Zhao, H. H. Kung and J. K. Lee, *J. Mater. Chem.*, **21**, 17325 (2011).
13. P. Poizot, S. Laruelle, S. Grugeon, L. Dupont and J.-M. Tarascon, *Nature*, **407**, 496 (2000).
14. H. Park, D. H. Yeom, J. Kim and J. K. Lee, *Korean J. Chem. Eng.*, **32**, 178 (2015).
15. P. Poizot, S. Laruelle, S. Grugeon and J. M. Tarascon, *J. Electrochem. Soc.*, **149**, A1212 (2002).
16. Y. He, L. Huang, J.-S. Cai, X.-M. Zheng and S.-G. Sun, *Electrochim. Acta*, **55**, 1140 (2010).
17. D. Pasero, N. Reeves and A. R. West, *J. Power Sources*, **141**, 156 (2005).
18. M. X. Liu, L. H. Gan, W. Xiong, Z. J. Xu, D. Z. Zhu and L. W. Chen, *J. Mater. Chem. A*, **2**, 2555 (2014).
19. X. M. Ma, L. H. Gan, M. X. Liu, P. K. Tripathi, Y. H. Zhao, Z. J. Xu, D. Z. Zhu and L. W. Chen, *J. Mater. Chem. A*, **2**, 8407 (2014).
20. M. X. Liu, X. M. Ma, L. H. Gan, Z. J. Xu, D. Z. Zhu and L. W. Chen, *J. Mater. Chem. A*, **2**, 17107 (2014).
21. H. J. Liu, S. H. Bo, W. J. Cui, F. Li, C. X. Wang and Y. Y. Xia, *Electrochim. Acta*, **53**, 6497 (2008).
22. R. Ryoo, S. H. Joo and S. Jun, *J. Phys. Chem. B*, **103**, 7743 (1999).
23. H. Zhang, H. Tao, Y. Jiang, Z. Jiao, M. Wu and B. Zhao, *J. Power Sources*, **195**, 2950 (2010).
24. H. S. Zhou, S. M. Zhu, M. Hibino, I. Honma and M. Ichihara, *Adv. Mater.*, **15**, 2107 (2003).
25. J. Gao, M. A. Lowe and H. D. Abruña, *Chem. Mater.*, **23**, 3223 (2011).
26. J. Jamnik and J. Maier, *Phys. Chem. Chem. Phys.*, **5**, 5215 (2003).
27. B. Sun, Z. Chen, H.-S. Kim, H. Ahn and G. Wang, *J. Power Sources*, **196**, 3346 (2011).
28. K. F. Zhong, X. Xia, B. Zhang, H. Li, Z. X. Wang and L. Q. Chen, *J. Power Sources*, **195**, 3300 (2010).
29. G. M. Zhou, D. W. Wang, F. Li, L. L. Zhang, N. Li, Z. S. Wu, L. Wen, G. Q. Lu and H. M. Cheng, *Chem. Mater.*, **22**, 5306 (2010).